Orbits

7

Thomas J.E. Muttikal, Prashant Raghavan,
Max Wintermark, Steven A. Newman,
and Sugoto Mukherjee

7.1 Introduction

This chapter describes the imaging characteristics of the more common orbital lesions. Although a specific imaging diagnosis of orbital pathology may not always be possible, a combination of clinical information and imaging features can enable a relatively short list of differential diagnoses to be formulated in most instances.

7.2 Anatomy

The orbit is a pyramidal-shaped cavity formed by seven bones. The roof is formed by the orbital process of frontal bone and the lesser wing of sphenoid. The floor is formed by the orbital plates of the maxilla, zygoma, and the palatine bone. The medial wall is formed by the frontal process of the maxilla, the lacrimal bone, and the gracile lamina papyracea of the ethmoid bone. The greater wing of sphenoid, the zygoma, and the zygomatic process of frontal bone form the lateral wall (Figs. 7.1, 7.2, and 7.3).

The contents of the orbit include the globe, the external ocular muscles (EOM), the optic nerve, cranial nerves III and IV, the first (ophthalmic, V1) division of V and VI, the ophthalmic artery, the superior and inferior ophthalmic veins, fat, the lacrimal apparatus, and the orbital septum (Figs. 7.1, 7.2, and 7.3).

The contents of the various channels of the orbit are summarized in Box 7.1.

7.3 Imaging Modalities

7.3.1 Ultrasound

Ultrasound of the orbit is best performed with a high-frequency linear transducer, ideally 10 MHz or higher. US is used to evaluate the eye and superficial structures and provides limited evaluation of deeper intraorbital structures. It is particularly useful when ophthalmoscopic examination is limited due to the presence of

P. Raghavan et al., *Manual of Head and Neck Imaging*,
DOI 10.1007/978-3-642-40377-4_7, © Springer-Verlag Berlin Heidelberg 2014

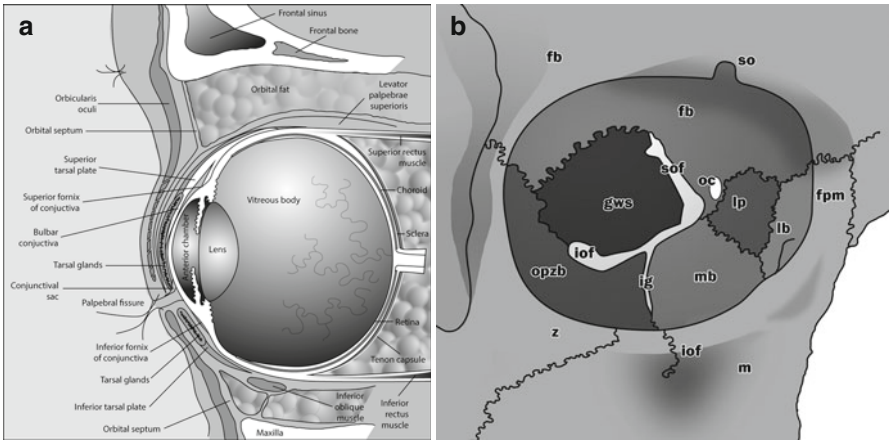

Fig. 7.1 Sagittal graphic (**a**) showing the gross anatomy of the globe and the orbit. Note the three layers of the globe consisting of retina, choroid, and sclera. The bony orbit (**b**) shows the relationships of the various foramina and fissures including the superior orbital fissure (*sof*), inferior orbital fissure (*iof*), and the optic canal (*oc*), as well as the superior (*sf*) and the inferior orbital foramina (*iof*). The bones forming the bony orbit include frontal bone (*fb*), greater wing of sphenoid (*gws*), orbital plate of the zygomatic bone (*opzb*), lacrimal bone (*lb*), frontal process of maxilla (*fpm*), supraorbital notch (*so*), infraorbital groove (*ig*), maxillary bone (*mb*), and lamina papyracea (*lp*). Other abbreviations in the figure include *m* maxilla, *z* zygomatic bone

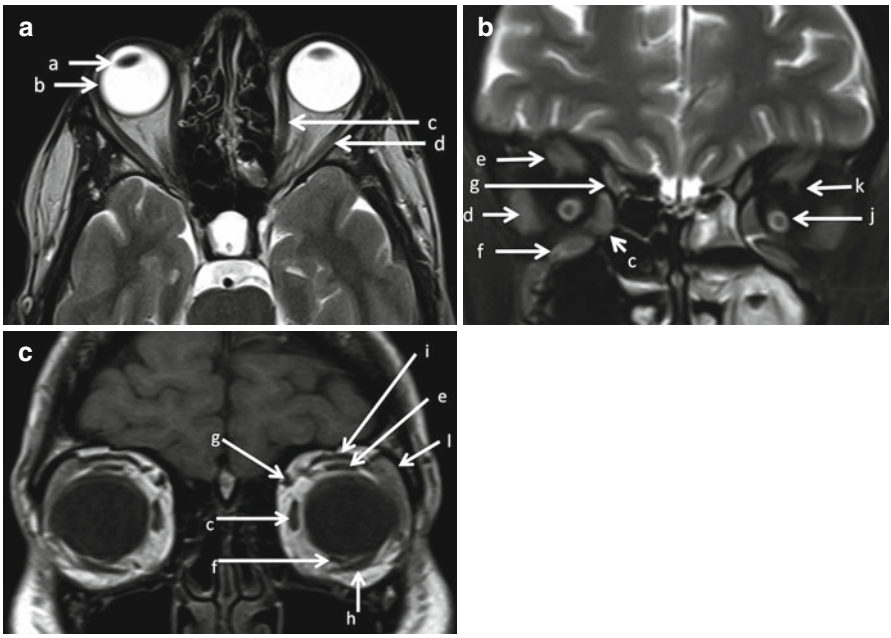

Fig. 7.2 Axial T2WI (**a**) and coronal T2WI with fat saturation (**b**) and coronal T1WI (**c**) show the easily identifiable intraorbital structures and extraocular muscles on MR. These include (*a*) lens, (*b*) globe, (*c*) medial rectus, (*d*) lateral rectus, (*e*) superior rectus, (*f*) inferior rectus, (*g*) superior oblique, (*h*) inferior oblique, (*i*) levator palpebrae superioris, (*j*) optic nerve sheath complex showing optic nerve surrounded by fluid in the optic nerve sheath, (*k*) superior ophthalmic vein, and (*l*) lacrimal gland

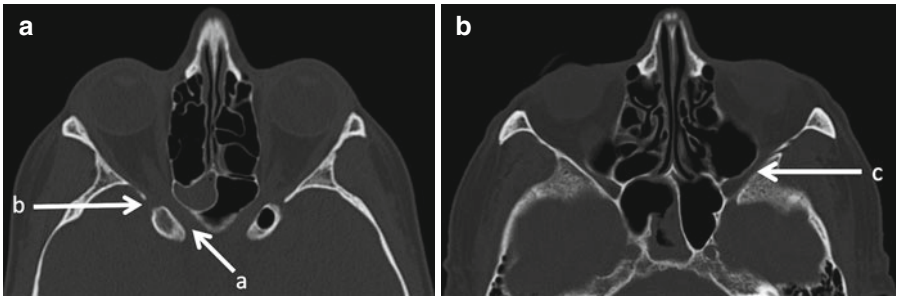

Fig. 7.3 Axial CT images (**a**, **b**) show the interrelationships of (*a*) optic canal, (*b*) superior orbital fissure, and (*c*) inferior orbital fissure

Box 7.1. Bony Channels of the Orbit

Optic canal	At apex of orbit, within the lesser wing of sphenoid bone	Optic nerve, ophthalmic artery with accompanying sympathetic fibers
Superior orbital fissure	Between the lesser and greater wings of the sphenoid	Branches of cranial nerves III, IV, and VI and cranial nerve VI, orbital branch of the middle meningeal artery, recurrent branch of the lacrimal artery and superior ophthalmic vein
Inferior orbital fissure	Between the greater wing of sphenoid, maxilla, and palatine bones	Maxillary nerve, zygomatic nerve, parasympathetics to lacrimal gland, infraorbital artery, infraorbital vein, and branch of inferior ophthalmic vein to pterygoid plexus

The infraorbital canal transmits the infraorbital nerve and vessels from the orbit to the face

opaque ocular media such as by cataract or vitreous hemorrhage. US is commonly performed by the ophthalmologist as an office procedure for evaluating a mass seen during ophthalmoscopy, to look for a mass underlying a retinal detachment, to evaluate ocular trauma, and for biometry. Color Doppler can be used to evaluate lesional vascularity.

7.3.2 Cross-Sectional Imaging

CT is the modality of choice in suspected orbital trauma, in orbital infection in the setting of sinusitis, and in the initial evaluation of an orbital mass. In patients with trauma, an unenhanced scan is sufficient. CT demonstrates bony changes and calcifications better than MRI. However, it must be employed judiciously in children and young patients where radiation exposure to the lens is a legitimate concern. CT scan and MRI can both provide complimentary information in the evaluation of orbital masses. A standard orbit MR study comprises of axial and coronal thin section unenhanced non-fat-suppressed T1-weighted images (the hyperintense fat provides excellent background contrast), a coronal fat-suppressed T2W sequence (for evaluating

Box 7.2. Multispatial Lesions

Lesion	T2	Pain	Additional helpful features
Plexiform neurofibroma	Hyperintense, central low intensity—target sign	Generally painless	Associated findings of NF1
Venous-lymphatic malformation	Heterogeneous, fluid-fluid levels	May be painful during thrombosis or sudden hemorrhage	
Orbital cellulitis	Hyperintense	Painful	Clinical features of infection
Orbital Pseudotumor	Hypointense	Painful	
Sarcoid	Hypointense	Generally painless	CNS or systemic sarcoidosis
Wegener	Hypointense	Generally painless	Other manifestation of Wegener, especially in nasal cavity and paranasal sinuses
Lymphoma	Hypointense	Painless	Restricted diffusion
Infantile hemangioma	Slightly hyperintense	Painless	

the optic nerve), and post-contrast fat-suppressed axial and coronal T1W images. CTA and MRA are useful when a vascular process such as a carotid-cavernous fistula or AV malformation is suspected.

The primary role of the radiologist is to precisely localize the lesion, estimate its site of origin and describe its extent. An attempt should be made to describe the lesion as focal or multispatial (Box 7.2), whether it involves intra or extraconal compartments, and its origin from the globe, optic nerve, lacrimal gland, vascular structures, extraocular muscles or the bony orbit.

7.4 Congenital/Developmental Anomalies

7.4.1 Coloboma

A coloboma is a focal discontinuity in the structure of the globe resulting from the failure of closure of the embryonic choroid fissure between the 5th and 7th weeks of life. Posterior colobomas, which include choroidoretinal, and optic disc colobomas are the more common type. They can occur as isolated lesions or as a part of a more widespread syndromic process. Isolated colobomas are usually unilateral, while

Fig. 7.4 Coloboma and lacrimal abscess. Axial contrast-enhanced CT scan showing incidental finding of coloboma of the right eye (*long arrow*). The patient was imaged for the left lacrimal gland abscess (*short arrow*)

syndromic forms tend to be bilateral. They appear as focal protrusions isodense to the vitreous on non-enhanced CT (NECT) scan and isointense to the vitreous of MRI, unless complicated by retinal detachment and hemorrhage (Fig. 7.4). A large coloboma may also present as an intraorbital cyst associated with a small globe (microphthalmia).

7.4.2 Persistent Hyperplastic Primary Vitreous

Persistent hyperplastic primary vitreous results from failure of regression of embryonic ocular blood supply. There are three types—posterior, anterior, and mixed. In posterior PHPV, there is an enhancing retrolental soft tissue with a stalk, representing the remnant of the primitive hyaloid artery, extending from the posterior surface of the lens to the head of the optic nerve (Fig. 7.5). Retinal detachment is frequently present and the globe is small. In anterior PHPV, the anterior chamber is shallow, the lens is thin and dysplastic, and an abnormal enhancing tissue is present in the region of the ciliary body and lens. The mixed type demonstrates features of posterior and anterior PHPV.

7.4.3 Coats' Disease

Coats' disease, seen in children, usually boys, under the age of ten, is caused by retinal telangiectasias and a leaky blood retinal barrier, which results in subretinal exudate accumulation. Coats' disease is usually unilateral and results in retinal detachment. The exudate appears hyperdense compared to vitreous on CT. The exudate, comprised mainly of cholesterol, is hyperintense on T1W MR images. Patients usually present with leukocoria and vision loss. The most important differential is retinoblastoma. On CT, the lack of calcification of the exudate of Coats enables differentiation from retinoblastoma. Also, post-contrast studies show no enhancement of the subretinal collection. Linear enhancement of the retinal detachment may however be present.

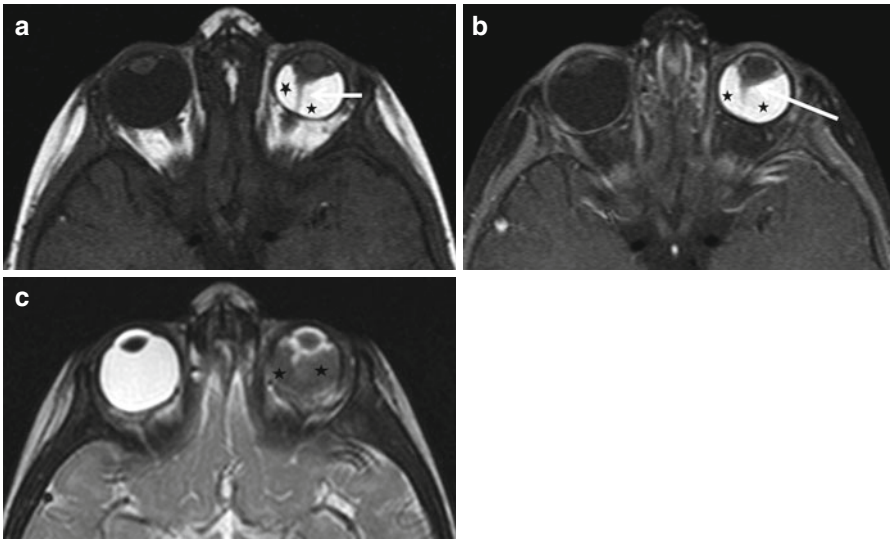

Fig. 7.5 Persistent hyperplastic primary vitreous (PHPV) in a 1-year-old patient. Axial T1 (**a**), axial fat-sat T1 post-contrast (**b**), and axial T2 (**c**) showing small left globe, stalklike hyaloid remnant extending from the posterior surface of the lens to the head of the optic nerve (*short arrow*), enhancing retrolental soft tissue (*long arrow*), and associated retinal detachment with hemorrhage (*black star*)

Box 7.3. Cystic Lesions

Dermoid
Epidermoid
Abscess
Venous-lymphatic malformation
Hemorrhage

7.4.4 Dermoids/Epidermoids

A dermoid is a congenital inclusion cyst occurring near suture lines, adjacent to the periosteum. The most common site is the superolateral portion of the orbit. Dermoid cysts commonly result in bony remodeling. They may be exophytic or endophytic. Exophytic cysts grow externally and are discovered early in childhood, while endophytic cysts grow internally and are encountered later in youth or early adulthood. Exophytic dermoids are usually small as they are identified earlier. Endophytic cysts are larger and may be associated with extensive bony changes. Other cystic lesions are summarized in Box 7.3.

They appear on unenhanced CT as well-defined fat density lesions (Fig. 7.6). The fat density is by no means universal, and it is not uncommon for them to present as fluid-containing lesions with no fat density. On MRI, the high T1 signal on fat,

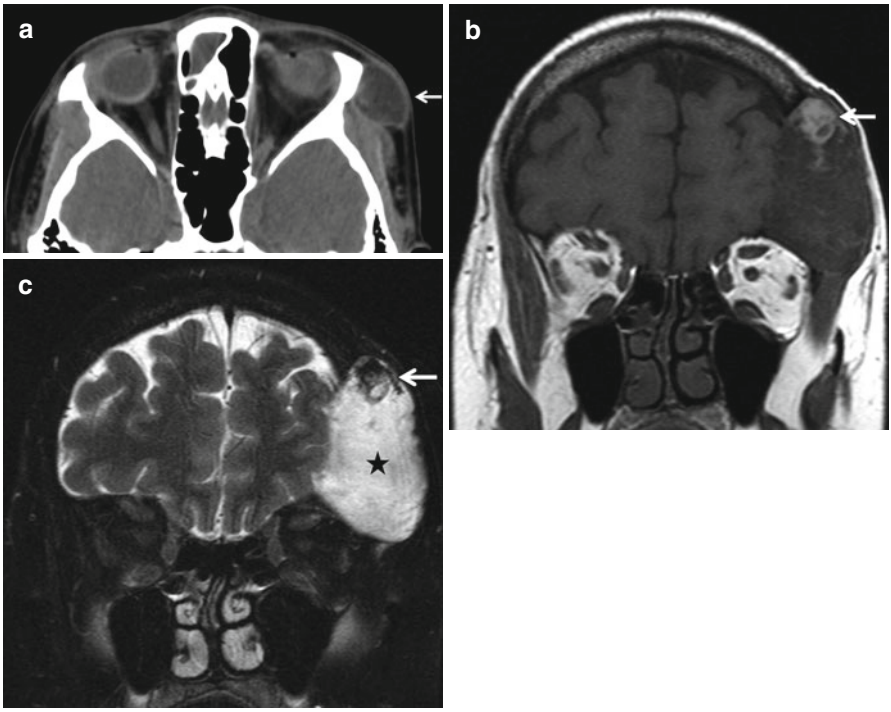

Fig. 7.6 Orbital dermoid. A 12-year-old patient presenting with gradually progressive, painless left periorbital swelling. Axial CT (**a**) showing cystic lesion without fat density along the superolateral margin of left orbit (*white arrow*). A 54-year-old patient, with long-standing history of left frontal swelling. Coronal T1WI (**b**) showing mixed signal intensity lesion with prominent fat nodule in its superior aspect (*white arrow*) with left frontal calvarial involvement. Coronal T2 fat-sat image (**c**) showing fat suppression in the superior nodular lesion (*white arrow*) and the hyperintense cystic component (*black star*). Compared to (a), this lesion is much bigger, with extensive lytic area in the frontal bone, related to the chronicity. The presence of fat within the lesion helps in diagnosis

when present, is characteristic. Occasionally a heterogeneous appearance due to intracystic debris may be encountered (Fig. 7.6). Sometimes, thin marginal enhancement on CT and MRI may be present. Irregular margins and perilesional inflammatory changes indicate rupture.

Epidermoid cysts demonstrate fluid signal/density on MRI and CT. A characteristic finding on MRI is restricted diffusion.

7.4.5 Neurofibromatosis Type 1

The ocular and orbital manifestations of NF1 include sphenoid wing dysplasia, plexiform neurofibroma, optic nerve glioma, buphthalmos, and optic nerve sheath ectasia. Sphenoid dysplasia, thinning, remodeling, or deficiency of the greater

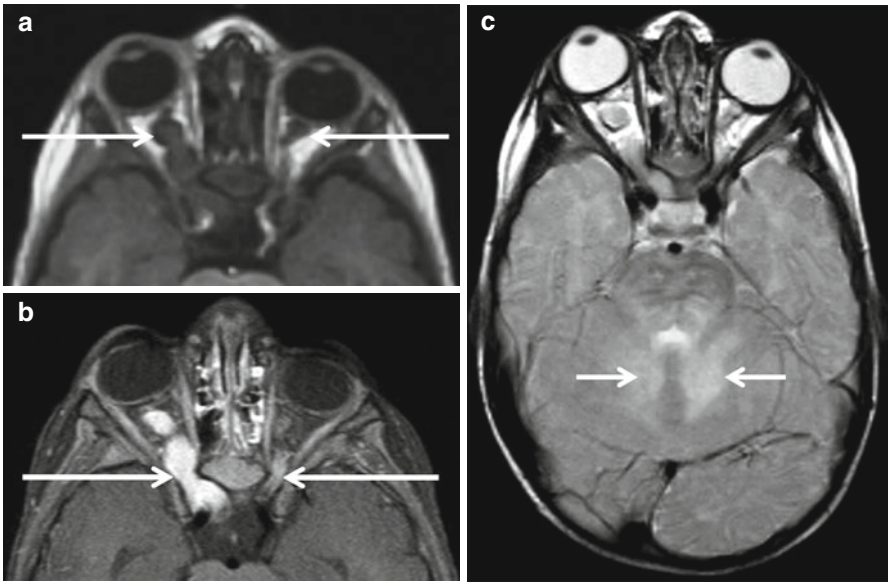

Fig. 7.7 Optic nerve gliomas in NF1. Axial T1-weighted images (**a**) showing bilateral optic gliomas (*long arrows*), right worse than left in a patient with NF1. Post-contrast axial T1 fat-sat image (**b**) shows enhancement of these lesions (*long arrows*). Axial T2-weighted sequences (**c**) show characteristic lesions of FASI (foci of abnormal signal intensity). These appear as non-enhancing foci of T2 prolongation and are thought to represent areas of myelin vacuolization (*short arrows* in **c**)

sphenoid wing, can result in the "bare orbit sign" on a frontal radiograph of the skull. Plexiform neurofibromas appear as variably enhancing infiltrative soft tissue masses on cross-sectional imaging. The target sign produced by foci of central T2 hypointensity is a typical finding. Perioptic dural sheath ectasia is an uncommon benign finding in patients with NF1. The distended CSF-filled sheaths are easily recognized on T2W MRI. Optic nerve gliomas are characterized by expansion of the nerve itself. They may be limited to the nerve or extend substantially along the visual pathway to involve the chiasm and hypothalamus (Fig. 7.7). They are low-grade neoplasms (pilocytic or fibrillary astrocytomas) and are frequently bilateral. No calcification is present on CT. They are of intermediate signal intensity and enhance variably on MRI.

7.5 Vascular Anomalies

7.5.1 Orbital Venous-Lymphatic Malformation (Lymphangioma)

Venous-lymphatic malformations are poorly marginated frequently trans-spatial multicystic lesions comprised of variable amounts of dysplastic lymphatic and venous elements. These lesions are best characterized on MRI. Cystic areas may show

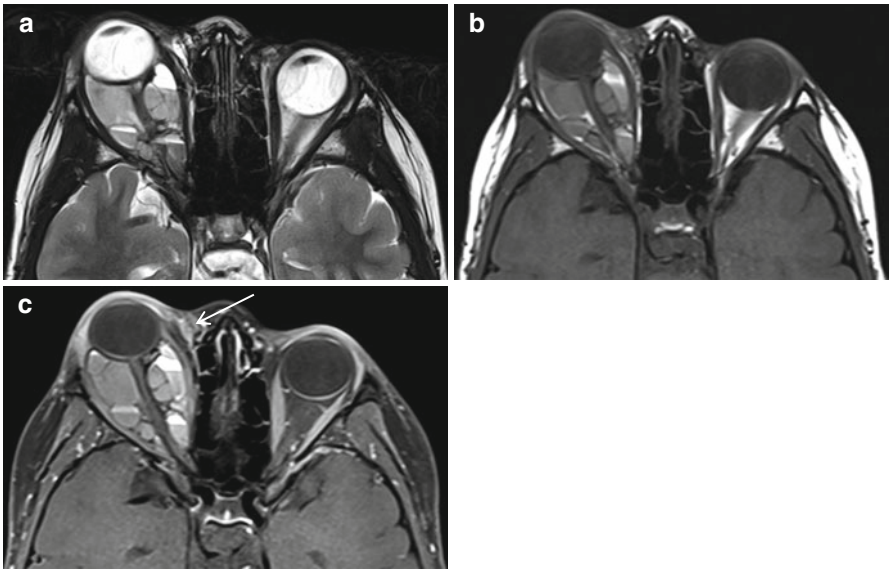

Fig. 7.8 Orbital venolymphatic malformation. Axial T2WI (**a**) showing complex multispatial lesion with multiple blood fluid levels in the right orbit in a 6-year-old patient. Axial precontrast TIWI (**b**) and post-contrast T1 fat-sat image (**c**) show a small enhancing portion (*arrow* in **c**) along the medial canthus of right eye

fluid-fluid levels and can contain blood products (Fig. 7.8). Enhancement is variable and is a function of the proportion of the venous component. Phleboliths, which appear on CT, as well-defined rounded calcific foci are a useful clue when present.

7.5.2 Venous Varix

An orbital venous varix is a distensible low-flow venous malformation connected with the systemic circulation. When large enough, it can result in intermittent reversible proptosis. Varices increase in size when systemic venous pressure increases, such as with coughing, straining, or compression of the jugular vein. Occasionally thrombosis, calcification, or hemorrhage can occur. Uncomplicated lesions appear as tubular soft tissue densities that enhance intensely with contrast. Patent varices can be made more conspicuous with the Valsalva maneuver. On MRI complex signal intensities due to slow flow and thrombosis may be present (Fig. 7.9).

7.5.3 Cavernous Hemangioma

Cavernous hemangiomas, the most commonly encountered orbital masses in adults, are vascular malformations comprised of endothelial-lined cavernous spaces with a

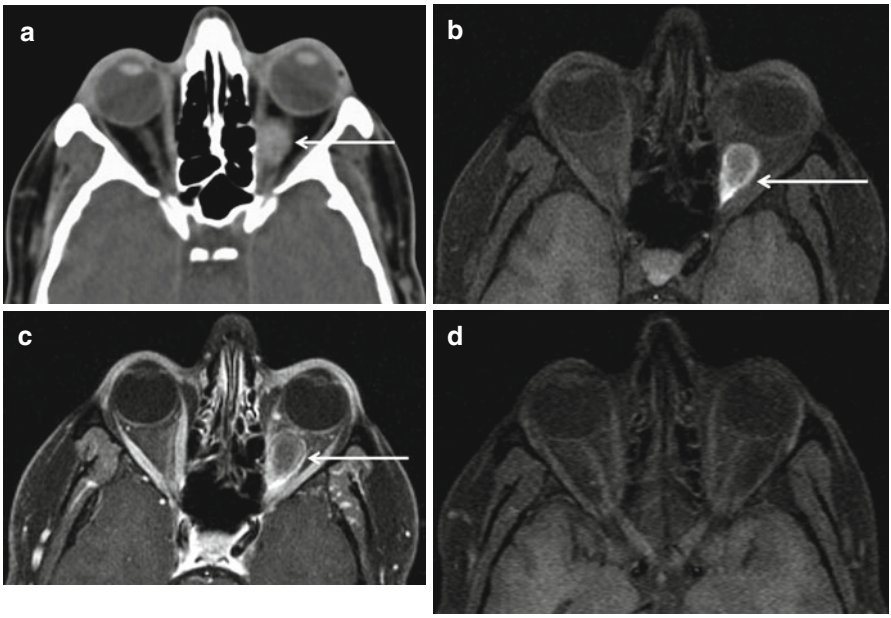

Fig. 7.9 Thrombosed venous varix. Axial CT scan (**a**) in this 42-year-old patient presenting with sudden onset left eye pain shows a well-defined hyperdense intraconal lesion (*arrow*). Axial T1 fat-sat image (**b**) also shows the T hyperintense intraconal lesion (*arrow* in **b**), without enhancement in post-contrast axial T1 fat-sat image (*arrow* in **c**). Follow-up axial T1 fat-sat image (**d**) after 3 months showing complete resolution of the lesion. The important pediatric lesions are summarized in Box 7.4

pseudocapsule of compressed normal orbital tissue. They are often incidentally detected on imaging but can present with slowly progressive painless proptosis. They are typically located in the intraconal compartment. They appear as well-defined homogeneous, noncalcified round or oval masses that exhibit progressive enhancement on delayed scans (Fig. 7.10).

7.6 Infectious and Inflammatory Disorders

The orbital complications of sinusitis are discussed in detail in Chap. 9.

These along with trauma and hemorrhage are the most common cause of acute proptosis (Box 7.5).

7.6.1 Idiopathic Orbital Inflammatory Disease

Idiopathic orbital inflammatory disease (orbital pseudotumor) is a poorly understood non-granulomatous steroid responsive disorder that can afflict any structure in the

Box 7.4. Pediatric Orbital Lesions

	Location	Important clinical feature	CT	MRI	Additional feature	DD
Dermoid	Occurs near the suture lines. Most common site is superolateral portion of orbit	Firm mass at the anterolateral portion of orbit	Bony remodeling is common. Fat density is seen in about ½ of the cases	Fat signal intensity seen in about ½ of the cases. Fluid-fluid level may be seen	If ruptured, appears irregular with adjacent inflammatory changes	Epidermoid has fluid density in CT and shows fluid signal intensity in MRI. Restricted diffusion in DWI differentiates it from dermoid
Venous-lymphatic malformation	Trans-spatial lesion	Gradually progressive proptosis, with intermittent worsening	Poorly marginated multicystic trans-spatial lesion. Calcification is rare	Fluid-fluid levels, varying blood signal intensity. Venous components and the periphery of cyst enhances		Orbital venous varix—dynamic change with Valsalva maneuver Orbital infantile hemangioma—intensely enhancing poorly marginated lesion with flow voids in MRI. Plexiform neurofibroma—infiltrative, variably enhancing lesion which appear hyperintense with central low intensity in T2-weighted imaging-target sign. Other features of NF1
Infantile hemangioma	Commonly preseptal, less commonly post-septal	Bluish skin discoloration with soft tissue mass	Lobular or infiltrative lesion	Flow voids	Imaging appearance changes with phase of involution, shows more fat content and septations	Orbital venous varix—dynamic change with Valsalva maneuver Plexiform neurofibroma Venolymphatic malformation Rhabdomyosarcoma—tendency to invade bone. Lack of flow void

(continued)

Box 7.4. (continued)

	Location	Important clinical feature	CT	MRI	Additional feature	DD
Optic glioma	Optic nerve	Decreased vision	Fusiform thickening, occasional hypodense cystic spaces	Fusiform thickening, occasional T2 hyperintense cystic spaces	May be associated with NF1 or sporadic	Optic nerve sheath ectasia can mimic optic glioma in NECT. Post-contrast imaging differentiates the two
Retinoblastoma	Arises from retina, extent depends on the tumor spread	White reflex	Calcifications in about 90 %	Hypointense in T2WI compared to vitreous. Noncalcified portion shows contrast enhancement	May have retinal detachment	Coats' disease—subretinal fluid collection, retinal detachment. No solid enhancing components Retinal astrocytic hamartoma resembles retinoblastoma radiologically. Association with tuberous sclerosis and neurofibromatosis helps to differentiate Ocular toxocariasis may show higher T2 signal intensity, which helps to differentiate. Calcification in CT is uncommon
Orbital rhabdomyosarcoma	Commonly extraconal, often contiguous with adjacent extraocular muscles	Painless proptosis	Bony erosion	T2 hyperintense		Orbital lymphoma—uncommon in children. Hypointense to isointense compared to EOM Orbital metastases can appear similar Plexiform neurofibroma—infiltrative, variably enhancing lesion which appear hyperintense with central low intensity in T2-weighted imaging-target sign. Other features of NF1

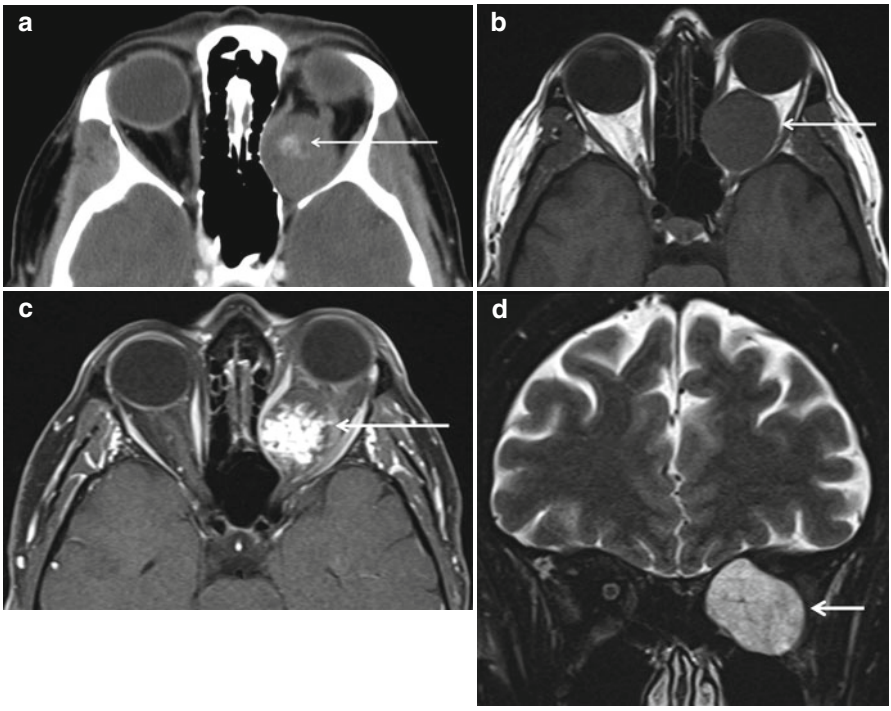

Fig. 7.10 Cavernous hemangioma. Axial CECT (**a**) showing central patchy enhancement in a well-defined intraconal lesion. In (**b** and **c**), the lesion is of intermediate signal intensity and enhances in a centripetal fashion. Coronal T2 fat-sat image (**d**) shows the characteristic T2 hyperintense nature of the lesion (*arrow*)

Box 7.5. Proptosis: Acute

Hemorrhage—hemorrhage in an underlying vascular lesion like venous-lymphatic malformation, trauma
Infection
CCF
Cavernous sinus thrombosis

orbit. IOID occurs in five forms—anterior (globe and retrobulbar soft tissues), lacrimal, myositic, apical (involvement of the orbital apex and cavernous sinus, Tolosa-Hunt syndrome), and diffuse and sclerosing (bilateral affliction of the orbits and paranasal sinuses) (Figs. 7.11 and 7.12). Painful unilateral ophthalmoplegia is the most common presenting feature. The myositic form, which on imaging is characterized by uniform enlargement of one or more extraocular muscles and their tendon sheaths, is the most frequently encountered variety of IOID. Involvement of the tendon sheaths is a typical finding in IOP and enables differentiation from thyroid ophthalmopathy, where despite smooth enlargement of the muscle belly, the tendon is unaffected. IOID may also occur as a diffusely infiltrative relatively T2

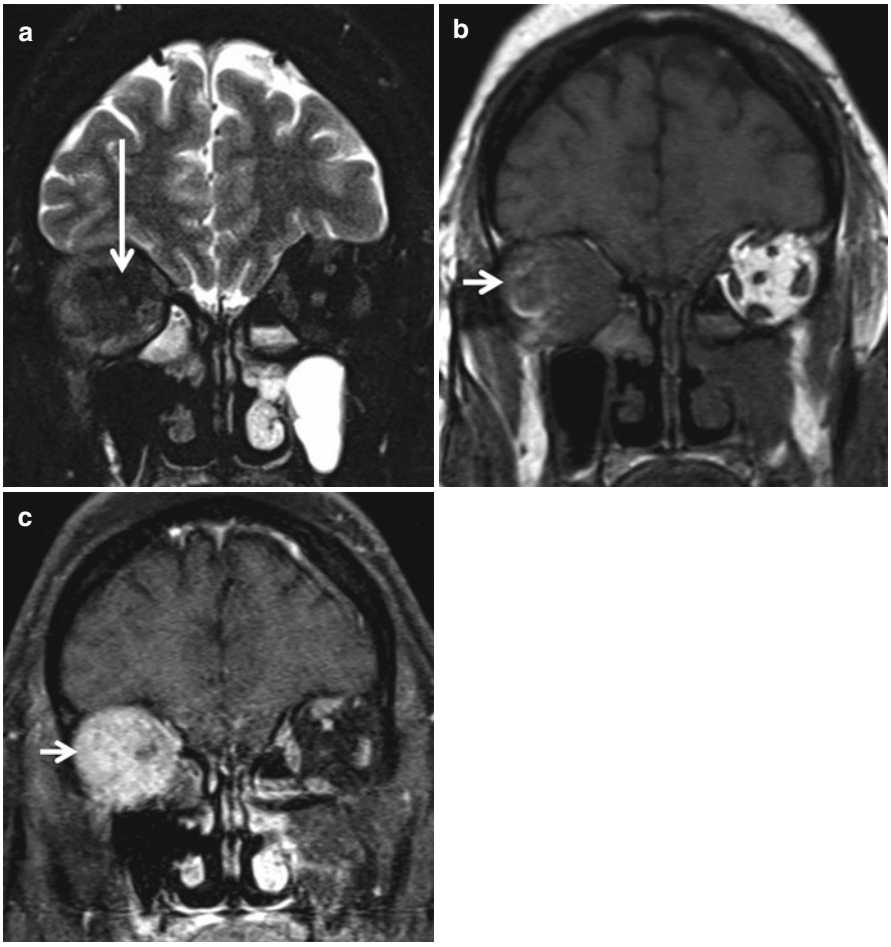

Fig. 7.11 Idiopathic orbital pseudotumor. Coronal T2 (**a**), precontrast T1 (**b**), and post-contrast T1 fat-sat (**c**) images, in a 42-year-old with painful slowly progressive proptosis, demonstrate an ill-defined T2 hypointense (compared to the extraocular muscles) (*long arrow* in **a**), enhancing lesion (*short arrow* in **b** and **c**) involving both the extra- and intraconal compartments. Typical features of this entity are T2 hypointensity on MRI, ocular pain and steroid responsiveness. These need not necessarily be present in every patient

hypointense enhancing process. When fibrosis is marked, the lesion may be profoundly T2 hypointense. Orbital lymphoma, sarcoidosis, and Wegener's granulomatosis can have very similar imaging appearances (Box 7.6), and one may have to rely on clinical data to arrive at the correct diagnosis. IgG4-related sclerosing disease is a type of orbital pseudotumor characterized by lymphoplasmacytic tissue infiltration with a predominance of IgG4-positive plasma cells, usually accompanied by fibrosis, and elevated serum levels of IgG4. IgG4-related sclerosing disease radiologically is indistinguishable from IOID.

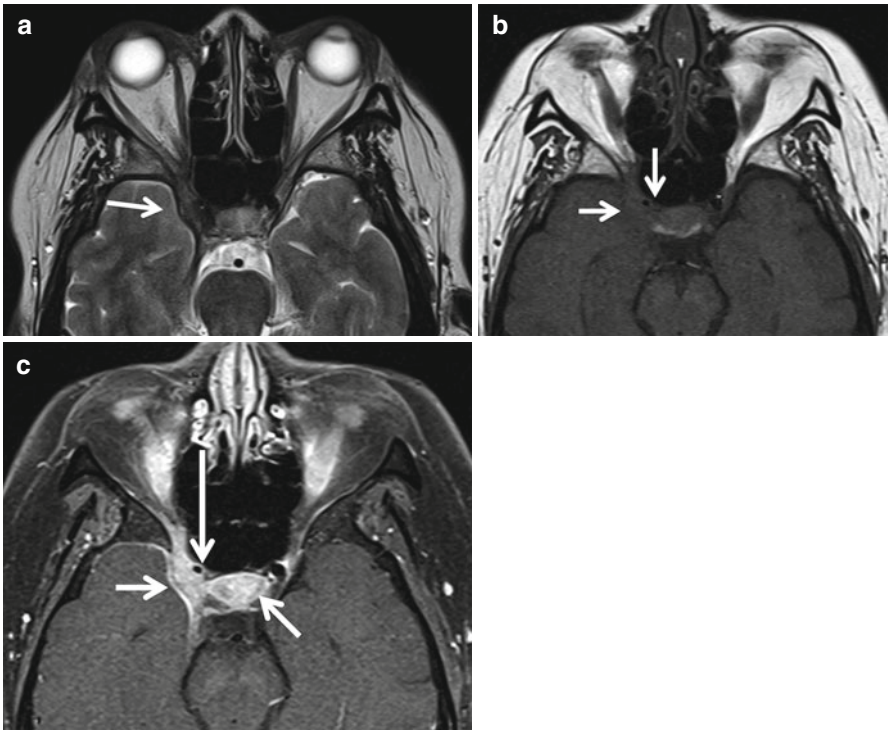

Fig. 7.12 Tolosa-Hunt syndrome in orbital pseudotumor. Axial T2 (**a**), precontrast T1 (**b**), and post-contrast fat-sat T1 images (**c**) demonstrate a T2 hypointense enhancing lesion (*short white arrows* in **a**–**c**) involving the right superior orbital fissure and the adjacent right cavernous sinus and sella. The right internal carotid artery is encased and narrowed by this lesion (*longer arrow* in **c**). This patient with an underlying diagnosis of orbital pseudotumor presented acutely with severe eye pain, headache, and external ophthalmoplegia

Box 7.6. Low T2 Signal Intensity Lesions

Orbital pseudotumor
Sarcoid
Wegener's granulomatosis
Lymphoma
Acute hematoma

7.6.2 Sarcoidosis

Although ophthalmological disease in sarcoidosis is frequent, imaging findings are uncommon. Anterior and posterior uveites are well-known phenomena associated with ocular sarcoid and are not evaluated with imaging. Soft tissue masses in the

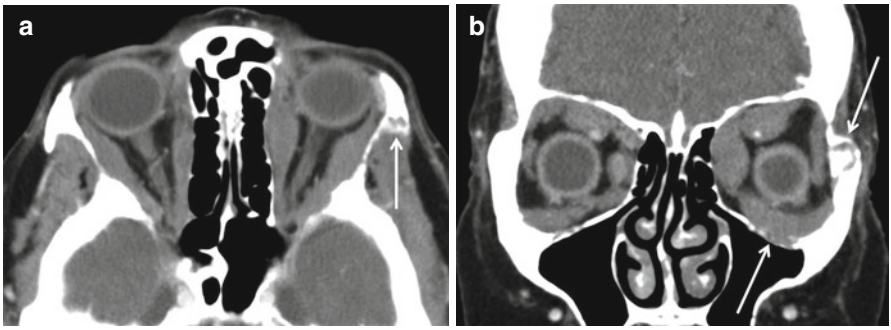

Fig. 7.13 Orbital sarcoidosis. Axial (**a**) and coronal (**b**) CECT in a 70-year-old woman presenting with gradual onset bilateral proptosis, showing bilateral enlarged external ocular muscles and bony lesions (*arrows*)

eyelids, lacrimal gland infiltration, optic nerve and sheath involvement, unilateral and bilateral retrobulbar soft tissue masses, extraocular muscle involvement, and, rarely, destructive osseous lesions have all been reported to occur (Fig. 7.13). There are no specific imaging features of orbital sarcoid, and often it is the presence of systemic disease elsewhere that points to the diagnosis.

7.6.3 Wegener's Granulomatosis

Imaging findings in Wegener's granulomatosis resemble that of sarcoidosis and IOID. Coexistent destructive sinonasal lesions are suggestive of WG, although such lesions may also be seen with sarcoidosis and IgG4-related inflammatory disease.

7.6.4 Thyroid Ophthalmopathy

Thyroid ophthalmopathy results from autoimmune orbital inflammation associated with Grave's disease. Thyroid ophthalmopathy, evident clinically as exophthalmos, may present before, during or after treatment of Grave's disease. Spindle-shaped smooth enlargement of the extraocular muscles, with sparing of the tendinous insertions, is typical of the disease. The inferior, medial, superior, and lateral rectus and oblique muscles are affected in decreasing order of frequency. These findings are usually bilateral and symmetric; however, they also may be unilateral. Additional findings include increased orbital fat, lacrimal gland enlargement, eyelid edema, stretching of the optic nerve, and tenting of the posterior globe. On CT the extraocular muscles are heterogeneous in appearance and contain foci of low density due to mucopolysaccharide deposition (Fig. 7.14). The enlarged muscles are isointense on T1WI and demonstrate increased signal intensity on fat-suppressed T2WI in the acute phase of the disease due to edema. In chronic thyroid ophthalmopathy, low signal intensity due to fibrosis may be present. Visual dysfunction may also occur due to compression of the optic nerve at the orbital apex by the enlarged

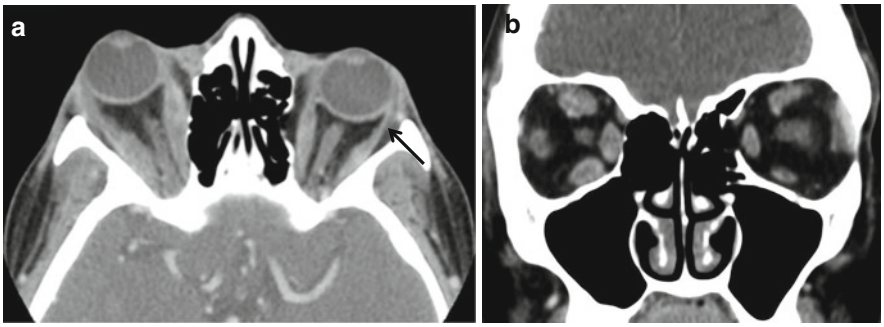

Fig. 7.14 Thyroid orbitopathy. Axial (**a**) and coronal (**b**) CT scan of a 43-year-old patient with thyroid orbitopathy showing bilateral enlarged external ocular muscles and characteristic sparing of the tendinous insertions (*arrow* in **a**). Note the tiny hypodensities within external ocular muscles in the coronal CT (**b**) due to deposition of mucopolysaccharides

Box 7.7. Extraocular Muscle Enlargement

Thyroid ophthalmopathy
Idiopathic pseudotumor
Malignancy—lymphoma, leukemia, metastases
Infectious myositis
Lymphoma, metastases
Vascular congestion—CCF, dural AV fistula, superior ophthalmic vein thrombosis

muscles. Lack of a cuff of fat around the nerve at the apex can indicate significant compression. The differential diagnosis of an enlarged extraocular muscle includes myositis pseudotumor, thyroid ophthalmopathy, and lymphoma (Box 7.7). Of these the only entity that spares the tendinous insertion is thyroid ophthalmopathy. Occasionally an EOM may be enlarged due to the presence of a metastatic deposit (usually from a lung, breast, or carcinoid primary); such enlargement is however nodular.

7.6.5 Optic Neuritis

Optic neuritis, best imaged with MRI, can occur due to a wide variety of infectious and inflammatory causes, including posttreatment (radiation-induced optic neuritis) (Figs. 7.15 and 7.16). The most common clinical scenario in which one encounters optic neuritis is in patients with multiple sclerosis (or with neuromyelitis optica), which is why it is prudent to scrutinize the entirety of the brain for demyelinating plaques. The inflamed nerve is hyperintense on fat-suppressed T2W images and enhances with gadolinium (Fig. 7.6). Occasionally, inflammation may be confined to the optic nerve head, when the term papillitis is used. There are no specific imaging patterns of optic neuritis.

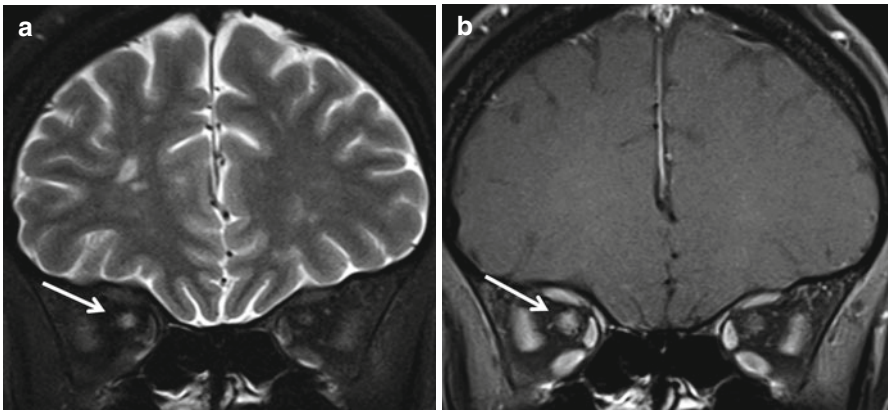

Fig. 7.15 Optic neuritis. Coronal T2 fat-sat image (**a**) showing enlarged hyperintense right optic nerve (*arrow*) in a 28-year-old patient with multiple sclerosis who presented with acute onset right-sided eye pain and vision loss. Post-contrast coronal T1 fat-sat image (**b**) showing abnormally enhancing enlarged right optic nerve (*arrow*)

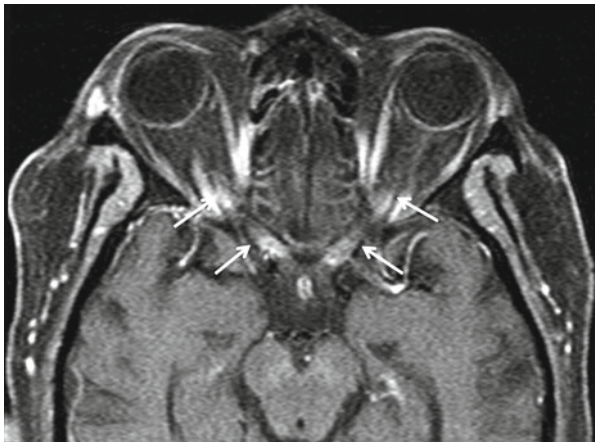

Fig. 7.16 Radiation-induced optic neuritis. Post-contrast axial T1 fat-sat image showing abnormally enhancing bilateral optic nerves (*arrows*) in this 54-year-old patient, following treatment for brain metastases

7.7 Benign Tumors

7.7.1 Infantile Hemangioma

Orbital infantile hemangioma is a benign vascular tumor, which usually appears within the first few weeks of life. Clinically, it presents as a mass with purplish discoloration of the eyelid/conjunctiva. Larger lesions may result in proptosis, diplopia, optic atrophy, and visual deterioration. Typical infantile hemangiomas grow during the first 1–2 years, stabilize, and regress spontaneously by late childhood. Most occur in the preseptal compartment. Infantile hemangiomas can appear lobular or infiltrative. Intense enhancement with intravenous contrast and prominent flow voids are a common feature (Fig. 7.17). Involuting hemangiomas can contain foci of fat and may not enhance intensely.

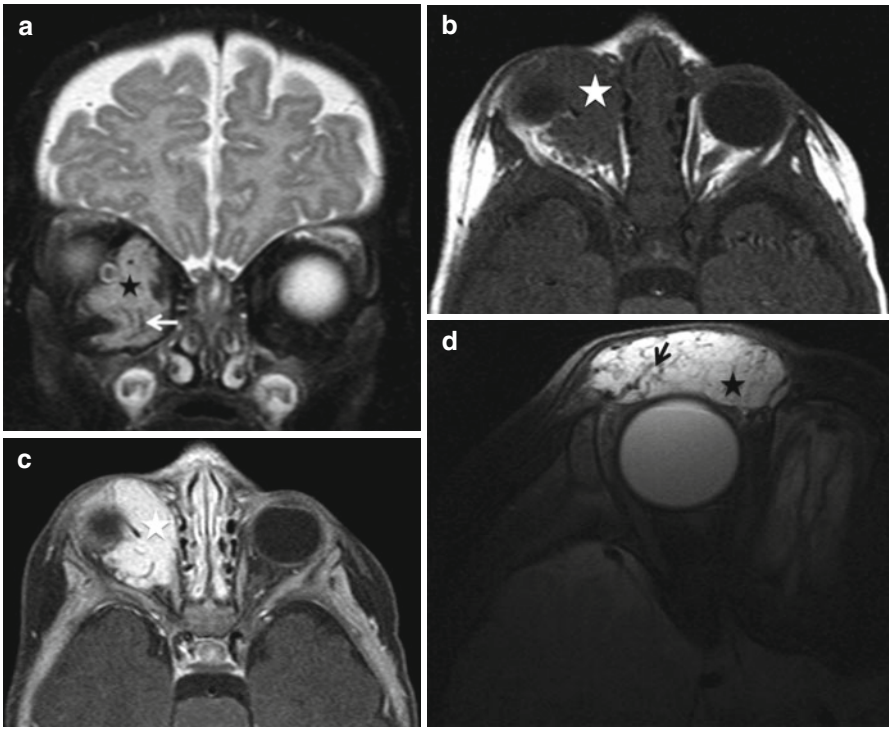

Fig. 7.17 Infantile hemangioma in a 3-month-old patient. Coronal T2 fat-sat image (**a**) showing hyperintense intraconal and extraconal irregular lesion (*star*) with flow voids (*white arrow*). Precontrast axial T1WI (**b**) shows the intermediate signal intensity of the lesion affecting preseptal and post-septal (intraconal and extraconal) compartments (*star*) with intense enhancement on the post-contrast axial T1 fat-sat image (**c**). Infantile hemangioma in another 3-month-old patient, with hyperintense lesion (*black star* in **d**) with prominent flow voids (*black arrow* in **d**) limited to the preseptal compartment

7.7.2 Optic Nerve Meningioma

Optic nerve meningiomas usually present with gradual painless, progressive vision loss. The occurrence of bilateral optic sheath meningioma is very rare and may be seen in patients with neurofibromatosis 2. They usually surround the optic nerve and grow in a tubular pattern. Occasionally a pedunculated or fusiform appearance may be present (Fig. 7.18). A linear "tram track" pattern of calcification is a typical finding (Fig. 7.18). Other lesions which can sometimes have a tram track pattern of enhancement are summarized in Box 7.8 below. They are best seen on post-contrast fat-suppressed MR images. Perioptic cysts representing trapped CSF in the optic nerve sheath, between the distal portion of the tumor and the globe may be present. Intracanalicular meningiomas represent a diagnostic challenge. They are difficult to identify and must always be actively sought for, when a patient, especially a female one, presents with painless gradual visual decline (Fig. 7.18).

Fig. 7.18 Optic nerve meningioma. A 58-year-old patient with gradual onset loss of vision of the right eye. Axial T1WI (**a**) showing intermediate signal intensity lesion near the orbital apex and in the optic canal (*arrow*). Post-contrast axial T1 fat-sat images (**b**) showing enhancing lesion which is predominantly involving the intracanalicular portion of optic nerve (*arrow*). These lesions can be missed unless specifically looked for in the dedicated contrast-enhanced fat-sat images. Coronal T2 fat-sat image (**c**) showing atrophy of the right optic nerve (*arrow*). (**d**, **e**) Optic nerve sheath meningioma. Another patient (**d**) with asymmetric enhancement along the intraorbital portion of right optic nerve (*arrow*), with atrophy of the optic nerve. Bilateral optic nerve sheath meningiomas with tram track calcification (*long arrow* **e**) in a different 53-year-old patient, who also had multiple intracranial calcified meningiomas (*short arrows*)

Box 7.8. Tram Track Enhancement

Meningioma
Perioptic neuritis
Optic neuritis
Lymphoma, leukemia, metastases
Sarcoid
Perioptic hemorrhage
Normal variant

7.7.3 Lacrimal Gland Benign Mixed Tumor

The typical appearance of a lacrimal gland pleomorphic adenoma is that of a well-defined lobulated variably enhancing mass with typical high signal on T2W images. Smooth bone remodeling may sometimes be present. Aggressive lacrimal masses such as lacrimal gland carcinomas show more irregular margins with local osseous invasion (Fig. 7.19).

7.8 Malignant Tumors

7.8.1 Retinoblastoma

Retinoblastoma is the most common intraocular childhood malignancy. Approximately 40 % of cases of retinoblastoma are due to heritable mutations, the rest being sporadic. Hereditary forms have an earlier age of onset, usually by 2 years of age and has propensity for bilateral and multifocal tumors. The nonheritable form is seen in older children and is typically solitary. Retinoblastomas result from inactivation of the retinoblastoma tumor suppressor gene on chromosome 13, at q14 locus. Although retinoblastomas can be visualized by direct ophthalmological examination, imaging plays an essential role in defining the extent of the disease (Box 7.9). Although USG, CT, and MRI are all used in the work-up in retinoblastomas, CT is ideally avoided due to concerns of increased long-term risk of malignancy. High-resolution MR imaging is the preferred modality to evaluate retinoblastomas.

On CT, the imaging findings are nonspecific, except for the appearance of calcification within the mass. Other calcified masses on CT include Coats' disease, retinal astrocytoma, phthisis bulbi, and ocular toxocariasis, all of which can be differentiated from retinoblastomas by a combination of clinical and imaging appearance.

On MR, retinoblastomas appear as heterogeneously enhancing lesions, with variable T1 (usually hyperintense to ocular fluid), with hypointense T2 signal (relative to vitreous) (Fig. 7.20a). Calcifications can be identified on either gradient echo MRI (GRE) or susceptibility-weighted imaging MRI (SWI) sequences (Fig. 7.20b). These lesions also restrict diffusion, although evaluation on this sequence can be limited due to susceptibility-related artifacts from calcifications. More importantly, MRI is done to precisely map the extent of the disease for accurate staging and management. Important intraocular findings to look for include presence of vitreous

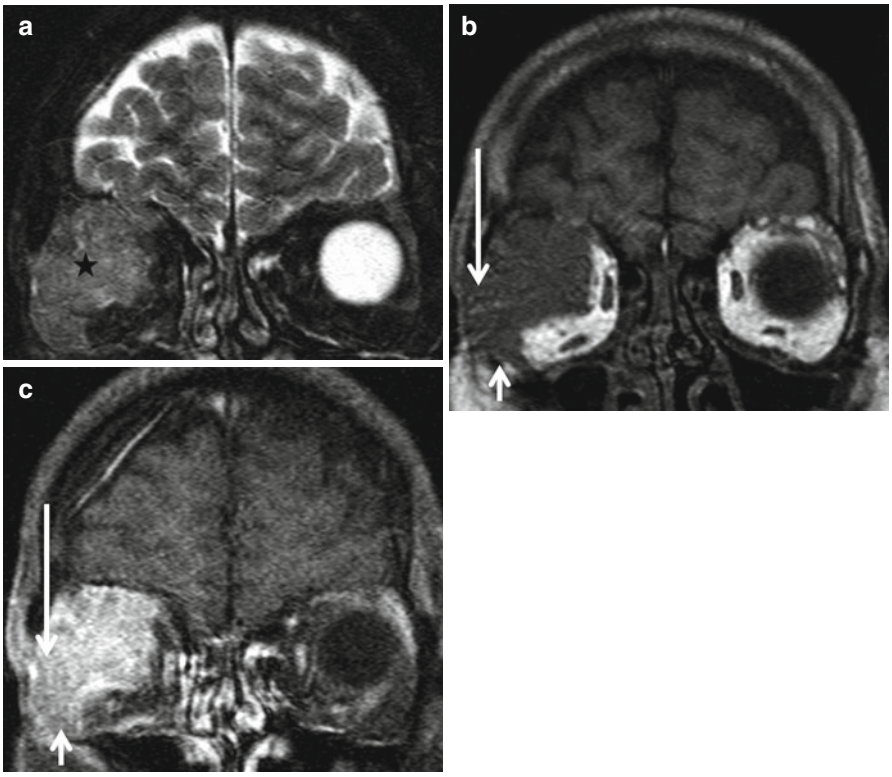

Fig. 7.19 Lacrimal gland carcinoma. Heterogeneous T2 hyperintense lesion (*star* in **a**), which demonstrates moderate enhancement on the precontrast T1 (**b**) and post-contrast T1 fat-sat images (**c**), with invasion of the lateral (*long arrow*) and inferior (*short arrow*) orbital bony walls. The bony destruction indicates that the lesion is aggressive, the location of the lesion being the only indication that the lesion may be arising from the lacrimal gland in the superolateral quadrant. The imaging appearance is nonspecific

Box 7.9. International Intraocular Retinoblastoma Classification

Group A	Tumors ≤3 mm in size, confined to retina, away from optic disc or foveola
Group B	Tumors ≥3 mm in size, confined to retina and close to optic disc or foveola
Group C	Localized (vitreous/subretinal) fine and limited seeding
Group D	Massive and/or diffuse intraocular seeding, retinal detachment
Group E	Larger tumors, with neovascular glaucoma, massive intraocular hemorrhage, anterior segment or ciliary body invasion or phthisis bulbi

Murphree AL (2005) Intraocular retinoblastoma: the case for a new group classification. Ophthalmol Clin North Am 18:41–53

seeding, retinal detachment, subretinal seeding, vitreous hemorrhage, anterior segment involvement, and choroidal/scleral invasion. Presence of vitreous hemorrhage (high T1 and low T2) may obscure tumor in MR imaging. In such cases, the tumor is usually best delineated by comparing precontrast and post-contrast T1 images.

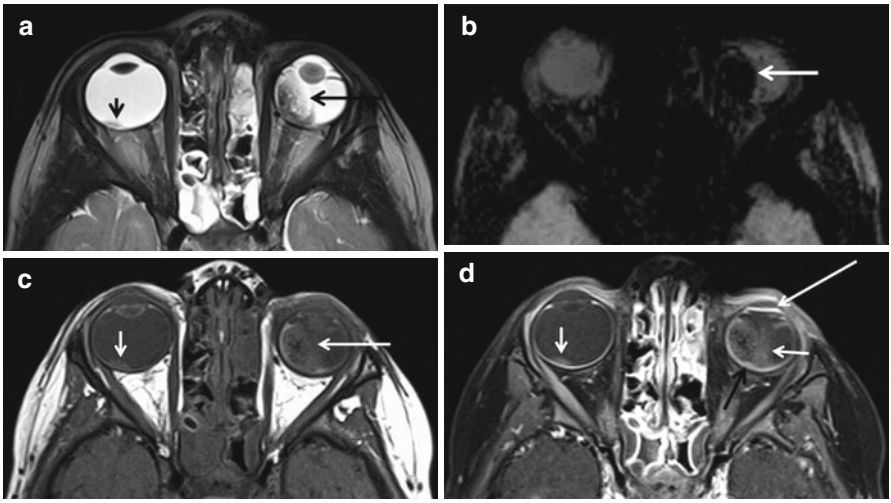

Fig. 7.20 Bilateral retinoblastoma. Axial T2 (**a**) and SWI (**b**) sequences demonstrate bilateral retinoblastomas. These appear as low signal intensity lesion in the left eye (*long black arrow*) and a small lesion in the right eye (*short black arrow*). The axial SWI (**b**) sequence nicely shows loss of signal with blooming, due to calcification within the lesion (*white arrow*) in the left eye. Axial TI sequences (**c**) shows heterogeneous hyperintensity of the lesions compared to the vitreous in the left eye (*long white arrow*) and a small lesion in the right eye (*short white arrow*). Contrast-enhanced T1 fat-sat image (**d**) showing enhancement of the lesions (*short white arrow*, *double white arrows*). Choroidal invasion is seen as focal thickening (*black arrow* in **d**). Plaque-like enhancement (*long white arrow* in **d**) of the iris is a reactive phenomenon (rubeosis iridis) and does not represent tumor spread

A potential pitfall is rubeosis iridis (the neovascularization of the iris), which appears as contrast enhancement within the anterior segment (Fig. 7.20d). This is not due to tumor spread, but is a reactive phenomenon mediated by vascular endothelial growth factors released by tissue hypoxia. Extraocular spread should be documented including extrascleral extension (abnormal enhancement of the retroorbital fat) and optic nerve involvement (whether pre- or postlaminar). However, MR has low sensitivity for predicting prelaminar optic nerve invasion. MR imaging findings of postlaminar optic nerve infiltration include focal optic nerve enhancement, with or without focal thickening of the optic nerve. Postlaminar optic nerve involvement indicates poor prognosis. MR can also document intracranial extension along optic nerve, leptomeningeal metastasis, and other primary intracranial tumors associated with bilateral retinoblastomas such as trilateral and quadrilateral retinoblastomas (pineal and suprasellar tumors).

7.8.2 Choroidal Melanoma

This is the most common primary intraocular tumor in adults. They are frequently asymptomatic or may sometimes present with painless visual disturbance. Rarely, they can result in retinal detachment. Choroidal melanomas appear as noncalcified

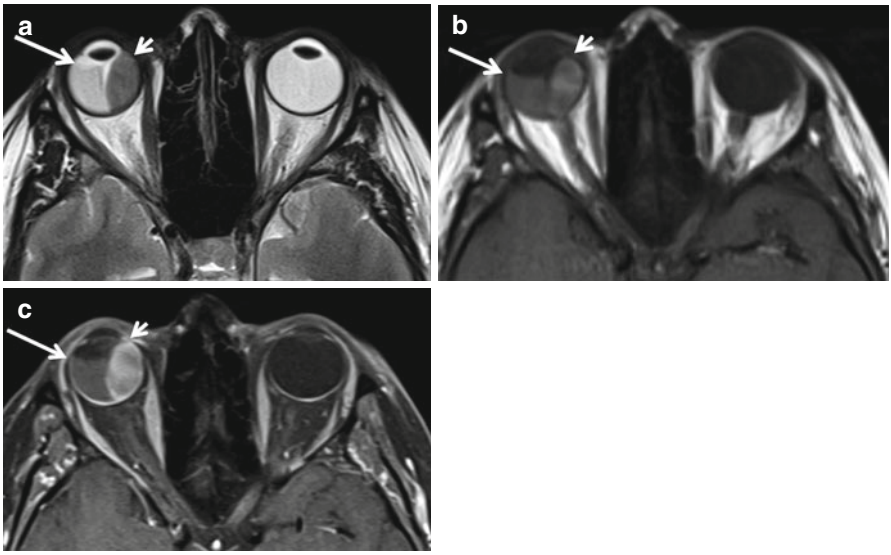

Fig. 7.21 Choroidal melanoma. Axial T2 (**a**) and T1 (**b**) sequences showing T2 hypointense (**a**), T1 hyperintense (**b**) lesion in the right eye (*short arrow*) with retinal detachment (*long arrow*). Post-contrast axial T1 fat-sat image (**c**) showing enhancing melanoma (*short arrow*) with non-enhancing retinal detachment (*long arrow*)

soft tissue masses on CT, with moderate enhancement. Depending on the melanin content, they can appear T1 hyperintense and T2 hypointense to the vitreous on MR, with moderate contrast enhancement (Fig. 7.21). Other choroidal masses such as metastasis can mimic the appearance of choroidal melanomas.

7.8.3 Orbital Rhabdomyosarcoma

Orbital rhabdomyosarcoma can be primary, arising from the primitive mesenchymal cells, or may represent secondary extension from extraocular muscles or from adjacent paranasal sinuses. These are typically found in pediatric patients and present with painless rapidly progressive proptosis and diplopia. The tumor can involve both the extra and intraconal compartments and frequently invades the bony orbit. On CT, the mass is usually mildly hyperdense with irregular enhancement. MR is helpful to delineate the entire extent of the lesion, which has treatment implications (Fig. 7.22).

7.8.4 Orbital Lymphoma

As with rhabdomyosarcomas, orbital lymphomas too can be primary or associated with systemic lymphomas. However, this is typically a disease of older patients,

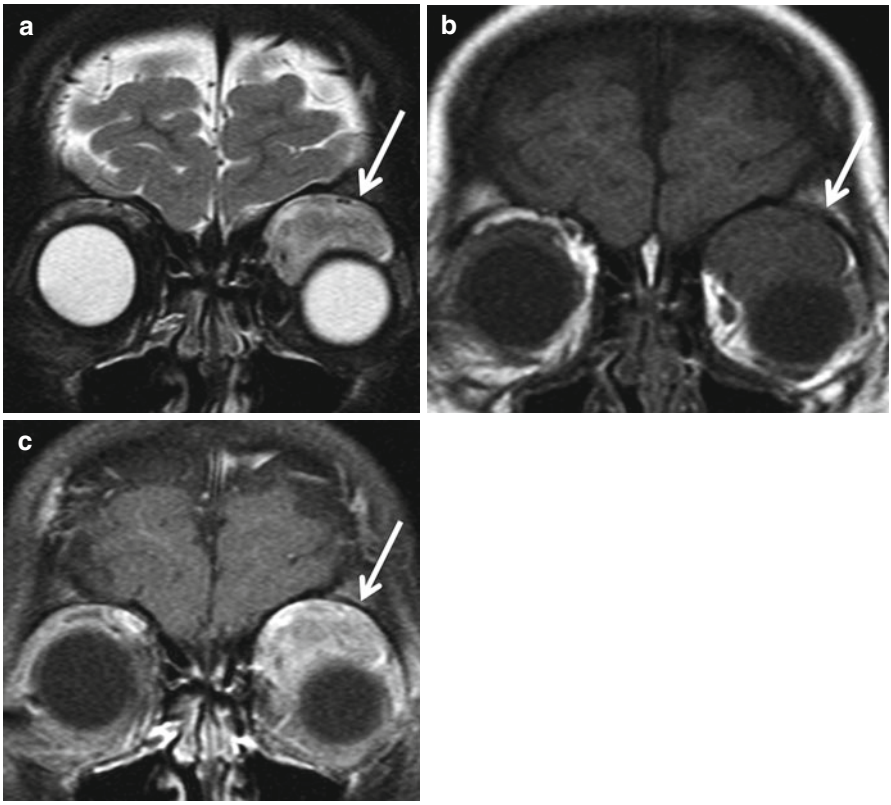

Fig. 7.22 Orbital rhabdomyosarcoma. Coronal T2 fat-sat images (**a**) in this 4-year-old patient showing heterogeneous hyperintense lesion in the superior aspect of the orbit (*arrow*), involving both the extraconal and intraconal compartments. The lesion shows intermediate signal intensity (*arrow*) in precontrast coronal T1 (**b**) with heterogeneous enhancement (**c**). Although the imaging appearance is nonspecific, the age of the patient helps in narrowing the differential diagnosis

who present with painless proptosis and diplopia. It can manifest as a unifocal lesion affecting any of the intraorbital structures or a diffusely infiltrative mass, like orbital pseudotumor. Unlike other aggressive intraorbital tumors, these lesions insinuate around the orbital structures without significant mass effect or osseous invasion (similar to orbital pseudotumors). Lymphoma may mimic thyroid ophthalmopathy by isolated involvement of the external ocular muscles. Orbital lymphomas appear isodense to hyperdense in NECT due to the hypercellularity of the tumor and show moderate contrast enhancement. On MR, these enhancing lesions are difficult to distinguish from orbital pseudotumor, because of similar imaging characteristics (Fig. 7.23). Diffusion-weighted imaging may help in differentiating these lesions, as lymphomas show restricted diffusion, due to their high cellularity (Fig. 7.23d, e).

7.8.5 Orbital Metastases

Metastatic disease to the globe is extremely uncommon. Usually, orbital metastases are either osseous or extraconal with secondary intraconal involvement. The

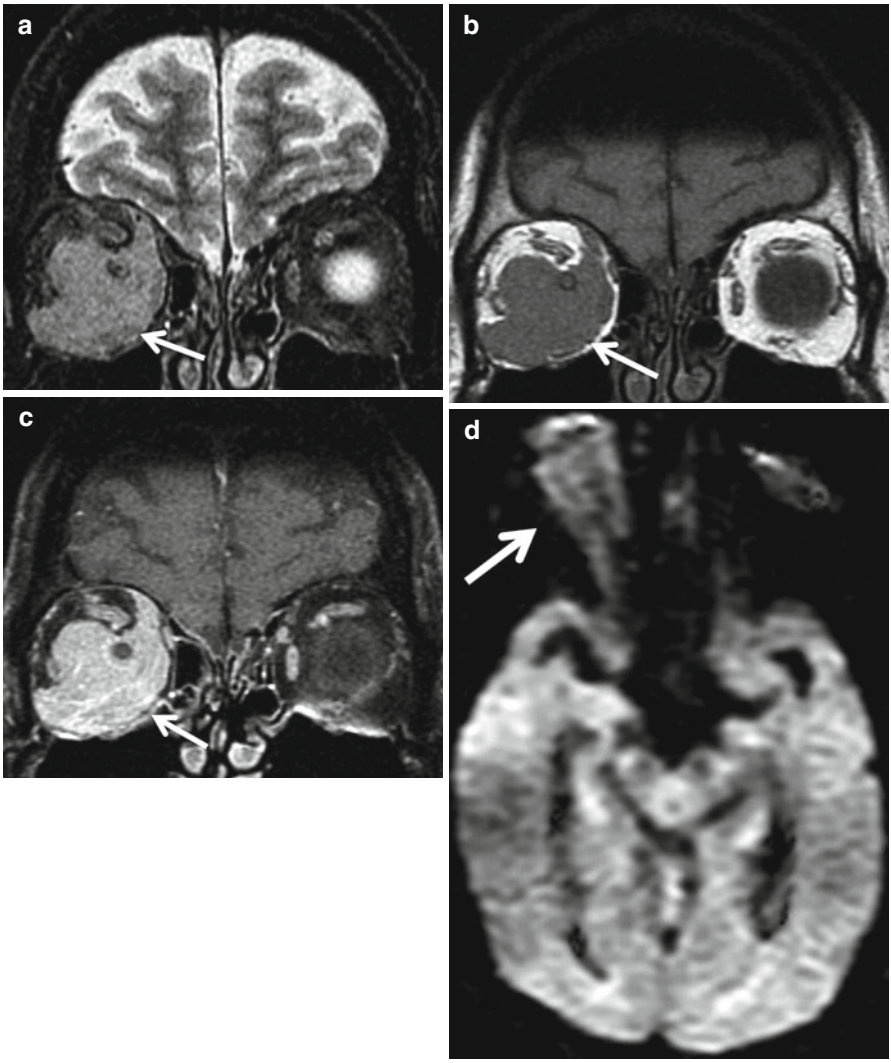

Fig. 7.23 Orbital lymphoma. Coronal T2 fat-sat image (**a**) showing slightly hyperintense infiltrative lesion (*arrow*) involving both the intraconal and extraconal compartments in this 62-year-old patient who presented with painless gradual onset proptosis. The lesion shows intermediate signal intensity in coronal T1 sequences (*arrow* in **b**) with intense contrast enhancement (*arrow* in **c**). The lesion also demonstrates restricted diffusion, (*arrows* in **d** and **e**). The absence of pain and restricted diffusion differentiates lymphoma from orbital pseudotumor

Fig. 7.23 (continued)

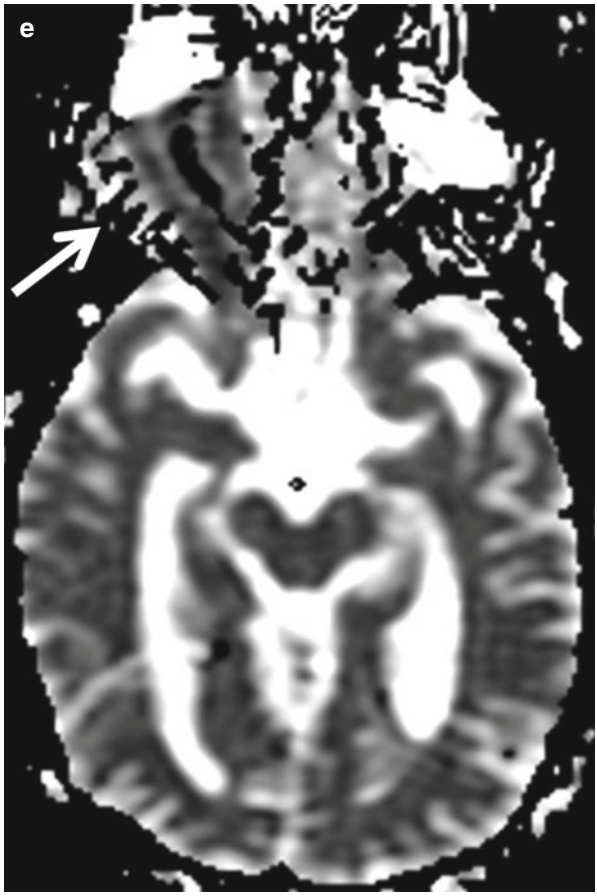

extraocular muscles are involved infrequently. More than half of the orbital metastasis is from breast and lung cancers. Although imaging findings are nonspecific, many of the metastatic lesions appear more nodular as compared to other mass lesions (Fig. 7.24).

7.9 Miscellaneous

7.9.1 Retinal Detachment

Retinal detachment refers to separation of the inner layers of the retina from the underlying retinal pigment epithelium. This results in crescent-shaped or V-shaped fluid collection on axial sections, with the apex converging at the optic disc. Retinal detachment can be spontaneous or due to underlying lesions, including tumors like retinoblastoma, choroidal melanoma, or metastases as well as other lesions such as

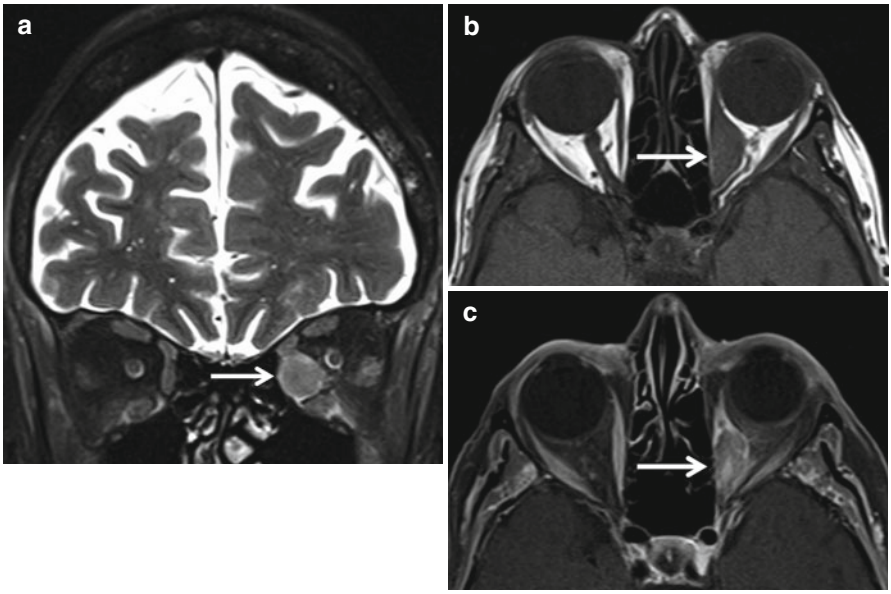

Fig. 7.24 Orbital metastases from breast cancer. Coronal T2 fat-sat image (**a**) showing slightly hyperintense lesion in left medial rectus (*arrow* in **a**). The lesion shows intermediate signal intensity in axial T1WI (*arrow* in **b**) with heterogeneous contrast enhancement (*arrow* in **c**)

trauma (due to subretinal hemorrhage), PHPV, and senile macular degeneration (Fig. 7.5).

7.9.2 Choroidal Detachment

Choroidal detachment is the separation of choroid from sclera with either serous or hemorrhagic collection, in the suprachoroidal space. These can be linear or crescentic and extend anteriorly to the ciliary bodies. Posterior extension is limited by the anchoring effect of short posterior ciliary arteries and nerves, thus sparing the posterior portion of the globe and the optic disc (unlike retinal detachments) (Fig. 7.25). Choroidal detachment can be seen with trauma, surgery, ocular hypotonia, and lesions such as choroidal melanomas.

7.10 The Surgeon's Perspective

The physical examination is a critical part of work-up for suspected orbital disease. This includes assessing the afferent visual pathways, including visual acuity, visual fields, and the presence of asymmetric optic nerve function as indicated by an afferent pupillary defect. Motility abnormalities suggesting involvement of the extraocular muscles or the cranial nerves innervating them are raised by the symptoms of

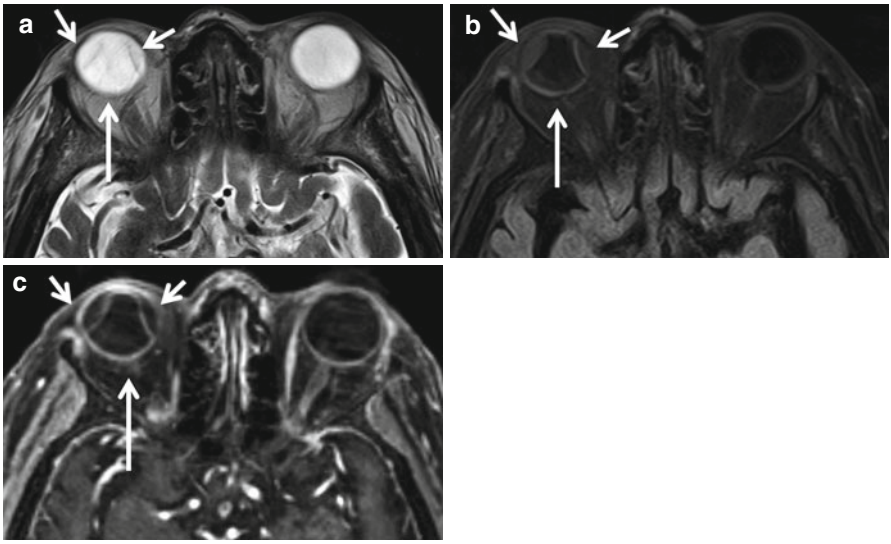

Fig. 7.25 Spontaneous choroidal detachment. Axial T2 (**a**), FLAIR (**b**), and post-contrast images (**c**) show the characteristic sparing of the posterior portion of the globe differentiating it from retinal detachment (*long arrow*). The subchoroidal fluid (*smaller white arrows*) appears hyperintense compared to vitreous in axial FLAIR (**b**)

diplopia and the findings of limited motility producing ocular malalignment. Most important to the suspicion of orbital pathology however remains, as recognized more than a thousand years ago, the presence of proptosis supplemented by abnormal lid position, resistance to retropulsion, sensory changes, and dystopia with the globe displaced in the direction opposite to the location of the lesion. More subtle findings on examination may include the presence of prominent episcleral vessels and increased intraocular pulse pressure suggestive of the presence of orbital venous hypertension, often related to carotid-cavernous fistula. Intermittent proptosis exacerbated by Valsalva maneuver may indicate the presence of an orbital venous varix.

Pathology affecting the orbit, like other locations in the body, may be congenital, developmental, inflammatory (including infectious), neoplastic, and vascular. Trauma can also affect the orbit, as can pathology arising from surrounding structures such as the paranasal sinuses and intracranially from the anterior and middle cranial fossae. Intracranial tumors that affect the orbit include most commonly meningiomas, particularly those arising from the sphenoid wing but occasionally from the floor of the anterior cranial fossa. Nasal or sinus tumors include adenocarcinoma, squamous cell carcinoma, undifferentiated carcinoma, esthesioneuroblastoma, and more rarely metastatic disease, melanomas, and adenoid cystic carcinoma. These secondary tumors are usually outlined and diagnosed by imaging and confirmed by endoscopic biopsy. Even with the most detailed history and physical examination, the specifics of localization and definitive diagnosis were usually impossible prior to the advent of imaging.

From the ophthalmologist's perspective, the most important aspect of localization on imaging is the lesions' relationship to the optic nerve. Not only does the location

suggest the optimal approach, rendering moot the conflict between whether transcranial or lateral orbitotomy is the ideal approach, in some cases, the specific characteristics of the pathology on imaging permit a diagnosis and thus suggest optimal treatment. Although other techniques, including the use of ultrasound, angiography, and venography, have been developed to play a supplementary role in the diagnosis of orbital pathology, CT and MR imaging remains the primary means of diagnosis and planning therapy in orbital disease. Imaging may also play a role in diagnosing intraocular pathology, but it usually is secondary to ophthalmoscopic evaluation and ultrasound.

Unlike intracranial pathology where MR proves superior in the majority of cases, in the orbit, CT and MR both remain extremely useful and often complimentary. Because of the contrast provided by the high fat signal intensity on CT scanning, it can often outline lesions within the orbit. As with other intracranial pathology, however, CT suffers at the bone-soft tissue interface, particularly at the orbital apex. There, especially when evaluating apical optic nerve pathology, MR offers a major advantage. CT is particularly sensitive to calcium and includes not only the bones around the orbit but also certain lesions that affect the globe including choroidal osteomas, scleral choristomas, and phthisis. While retinoblastoma often calcifies, these patients should probably not be studied with CT due to the risk of radiation-induced secondary tumors (often sarcomas) in patients with mutations in the RB1 (a tumor suppressor) gene. Retinoblastoma patients should avoid radiographic studies if possible (a combination of ultrasound and MRI are often adequate).

Soft tissue characteristics are better seen on MRI, and CT is superior for suspected foreign bodies with the possible exception of wood. Currently localization information provided by imaging includes involvement of the globe, the optic nerve, or the extraocular muscles. The pattern, whether it is infiltrative or well separated from the surrounding normal tissue, involvement of the surrounding bone provides additional information, while additional techniques may continue to provide supplementary information. One unusual characteristic of MR findings that could be helpful with orbital pathology is that of the paramagnetic features of melanin, meaning that instead of being bright on T2, melanomas are often dark on T2 and bright on T1. In orbital pathology more than any other location, imaging study remains the foundation upon which we make a diagnosis and decide on treatment.

While imaging studies are the backbone of orbital evaluation, it is far better to tailor our approach to lesions affecting the orbit based on pathology. Not all lesions need to be operated on. Malignant lesions are rarely curable with surgery and biopsy may direct treatment to radiation therapy or chemotherapy (particularly with lymphoproliferative lesions). Inflammatory or infectious pathology conversely needs to be treated with appropriate antibiotics or anti-inflammatories and other than drainage with as little surgery as possible. While specific diagnosis can sometimes be made on imaging, often tissue biopsy or cytology provided by fine needle aspiration may be necessary. Knowledge of the natural history, as provided by follow-up quantitative imaging studies supplemented by additional information including genetic testing and histopathology, provided either by biopsy or even by cytology from fine needle aspiration (especially when combined with flow cytometry,

immunohistochemical marking, and gene rearrangement studies), permits increasingly sophisticated decision making regarding orbital pathology. Although largely supplemental, ultrasound does have certain situations where it is particularly diagnostic, such as the "T sign" in patients with posterior scleritis.

It is impossible to maintain a practice in orbital pathology without a firm understanding of the role of the myriad imaging techniques now available. Ophthalmologists are encouraged to personally involve their radiologists to optimize the information obtained permitting better planning and results in taking care of patients with orbital lesions.

Further Reading

Chung EM, Smirniotopoulos JG, Specht CS et al (2007) Pediatric orbit tumors and tumorlike lesions: nonosseous lesions of the extraocular orbit. Radiographics 27:1777–1799

Gentry LR (1998) Anatomy of the orbit. Neuroimaging Clin N Am 8(1):171–194

Levin AV (2003) Congenital eye anomalies. Pediatr Clin North Am 50:55–76

Rauscheker AM, Patel CV et al (2012) High-resolution MR imaging of the orbit in patients with retinoblastoma. Radiographics 32(5):1307–1326

Smoker WR, Gentry LR, Yee NK et al (2008) Vascular lesion of the orbit: more than meets the eye. Radiographics 28:185–204